

Supporting Information

Dramatic Impact of the Lattice Solvent on the Dynamic Magnetic Relaxation of Dinuclear Dysprosium Single-Molecule Magnets

Wan-Ying Zhang,^a Yi-Quan Zhang,^c Shang-Da Jiang,^b Wen-Bin Sun,^{a,*} Hong-Feng Li,^a Bing-Wu Wang,^{b,*} Peng Chen,^a Peng-Fei Yan,^{a,*} and Song Gao^{b,*}

^aKey Laboratory of Functional Inorganic Material Chemistry Ministry of Education, School of Chemistry and Material Science Heilongjiang University, 74 Xuefu Road, Harbin 150080, China. E-mail: wenbinsun@126.com and yanpf@vip.sina.com

^bBeijing National Laboratory of Molecular Science State Key Laboratory of Rare Earth Materials Chemistry and Applications, College of Chemistry and Molecular Engineering, Peking University, Beijing 100871, China. E-mail: wangbw@pku.edu.cn and gaosong@pku.edu.cn

^cJiangsu Key Laboratory for NSLSCS, School of Physical Science and Technology, Nanjing Normal University, Nanjing 210023, China. E-mail: zhangyiquan@njnu.edu.cn

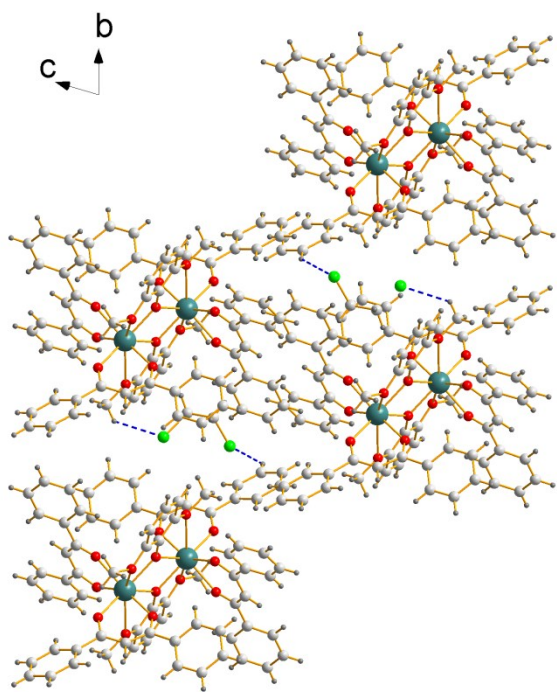


Fig. S1 Crystal packing of **2** along the *a*-axis.

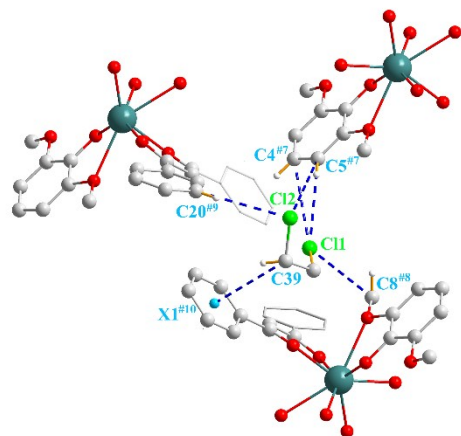


Fig. S2 Views showing the C-H...pi interactions and intermolecular Cl...H-C interactions among the crystallographically equivalent Dy-DMOP units of **2** (hydrogen atoms have been omitted for clarity; symmetrycodes: #7: $x, y-1, 1+z$; #8: $-x, 1-y, 1-z$; #9: $1-x, -y, 1-z$; #10: $x, y, z+1$).

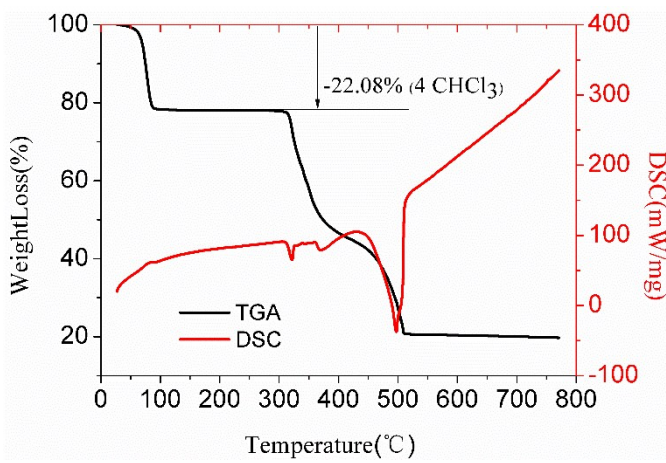


Fig. S3 TG curve of complex **1**.¹

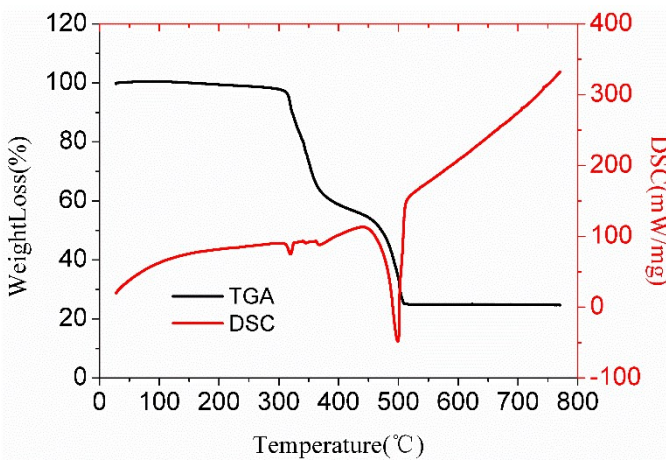


Fig. S4 TG analysis of complex **de1**.

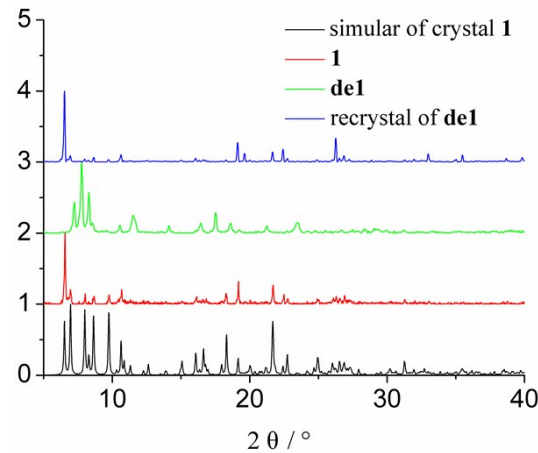


Fig. S5 PXRD patterns for complexes **1**, **de1** and the recrystallization of **de1**.

¹ Thermal analysis of **1** performed in air atmosphere at the heating rate of $10\text{ }^{\circ}\text{C min}^{-1}$ shows a weight loss of 22.1% in the temperature range $30\text{-}90\text{ }^{\circ}\text{C}$, close to the calculated value for releasing four lattice CHCl_3 molecules (calcd. 23.8%).

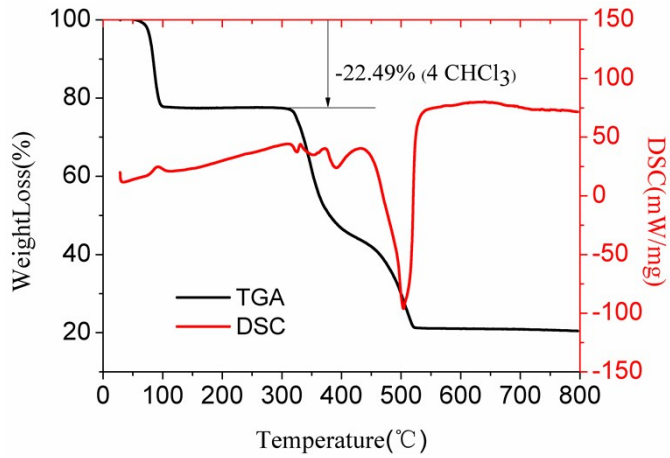


Fig. S6 TG analysis for recrystallization of **de1**.

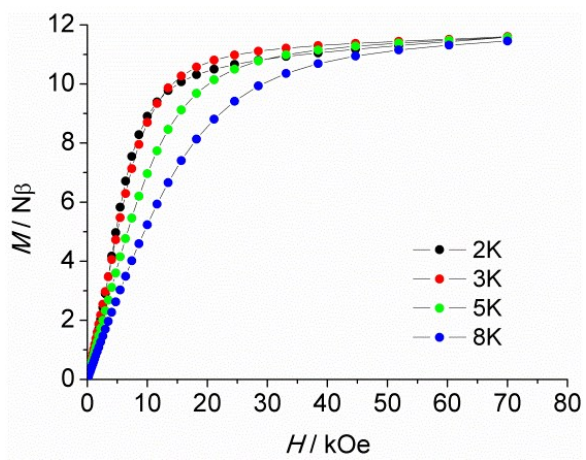


Fig. S7 Field dependence of the magnetization between 2 and 8 K for **1**.

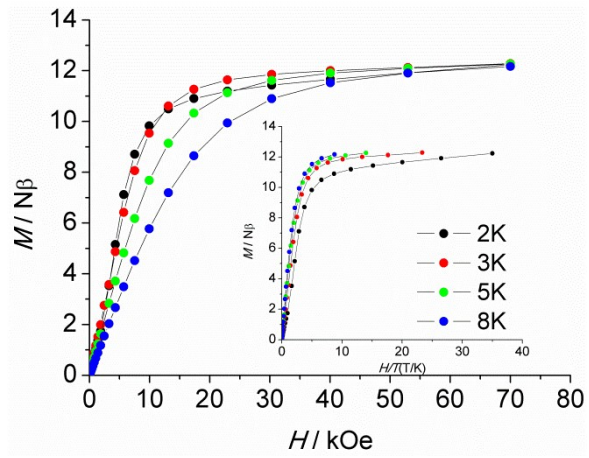


Fig. S8 Field dependence of the magnetization between 2 and 8 K for **2**.

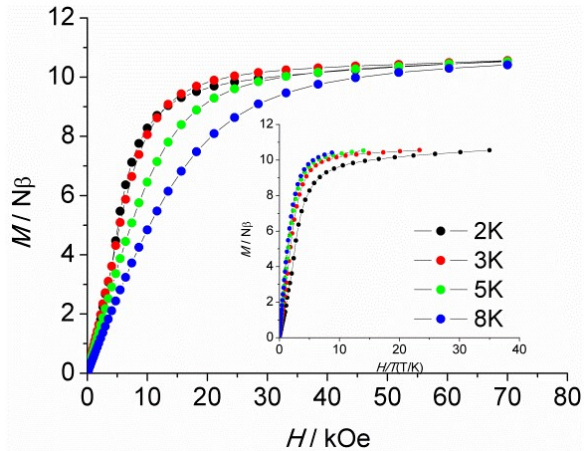


Fig. S9 Field dependence of the magnetization between 2 and 8 K for **de1**.

The $\chi_M T$ value of the Gd(III)_2 complex is $16.29 \text{ cm}^3 \text{ K mol}^{-1}$ at 300 K, somewhat smaller than the expected value $15.82 \text{ cm}^3 \text{ K mol}^{-1}$ of two uncoupled ${}^8S_{7/2}$ centers. With the known isotropic interaction, the Hamiltonian $H = \frac{2}{3}JS_{\text{Gd}1}\cdot S_{\text{Gd}2}$ results in the formula for the temperature dependence of the molar magnetic susceptibility in eqn (S1)^{S1,2}, where g is the Landé factor, β is the Bohr magneton, N is the Avogadro number, and k is the Boltzmann constant and $x = \frac{2J}{kT}$.

$$\chi_M T = \frac{2N g^2 \mu_B^2 e^x + 5e^{3x} + 14e^{6x} + 30e^{10x} + 55e^{15x} + 91e^{21x} + 140e^{28x}}{k(1 + 3e^x + 5e^{3x} + 7e^{6x} + 9e^{10x} + 11e^{15x} + 13e^{21x} + 15e^{28x})} \quad (\text{S1})$$

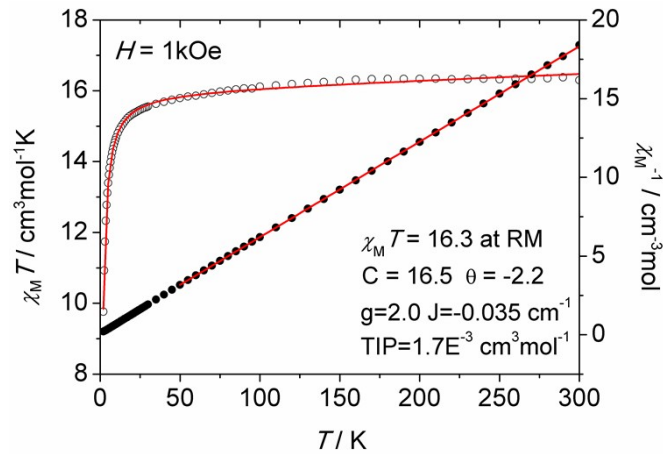


Fig. S10 Temperature dependence of $\chi_M T$ (open squares) and χ_M^{-1} (filled circles) for the complex **4**; the solid line represents the best-fit calculated values.

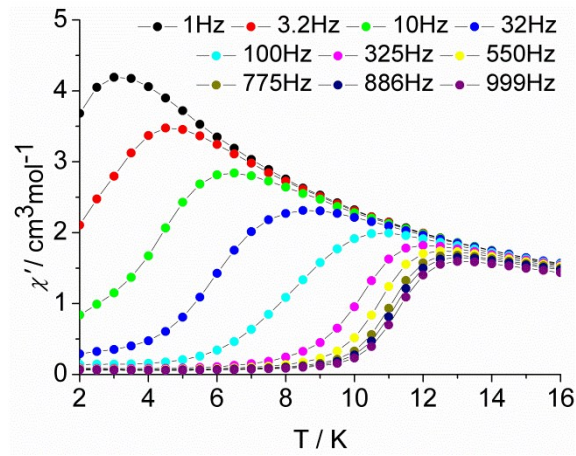


Fig. S11 Temperature dependence of the in-phase χ' ac susceptibility signals under zero dc field for **1**.

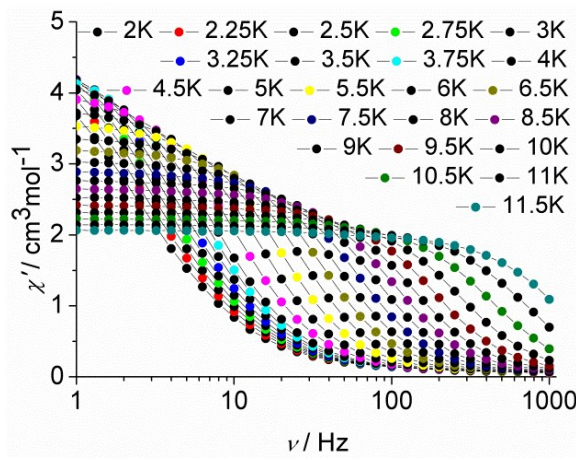


Fig. S12 In-phase susceptibility χ' vs frequency ν (logarithmic scale) in the temperature range 2-12 K for **1**.

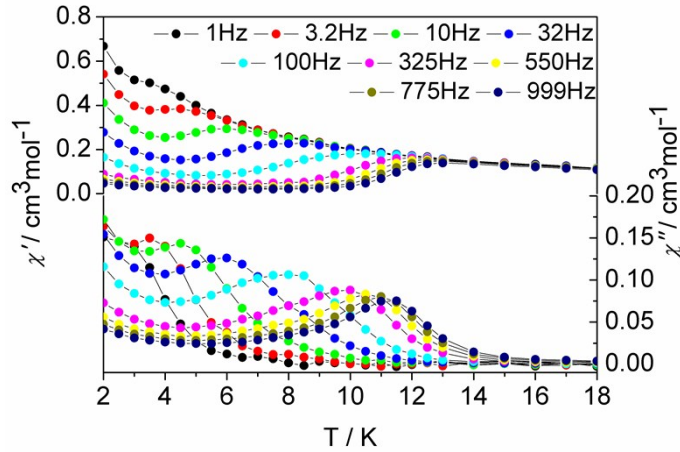


Fig. S13 Temperature dependence of the in-phase (χ') and out-of-phase (χ'') ac susceptibility signals under zero dc field at indicated temperatures for **1b**.

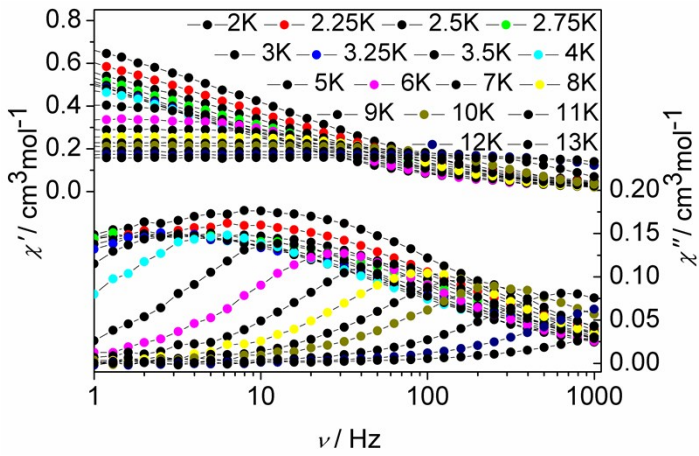


Fig. S14 Frequency dependence of the in-phase (χ') and out-of-phase (χ'') ac susceptibility signals under zero dc field at indicated temperatures for **1b**.

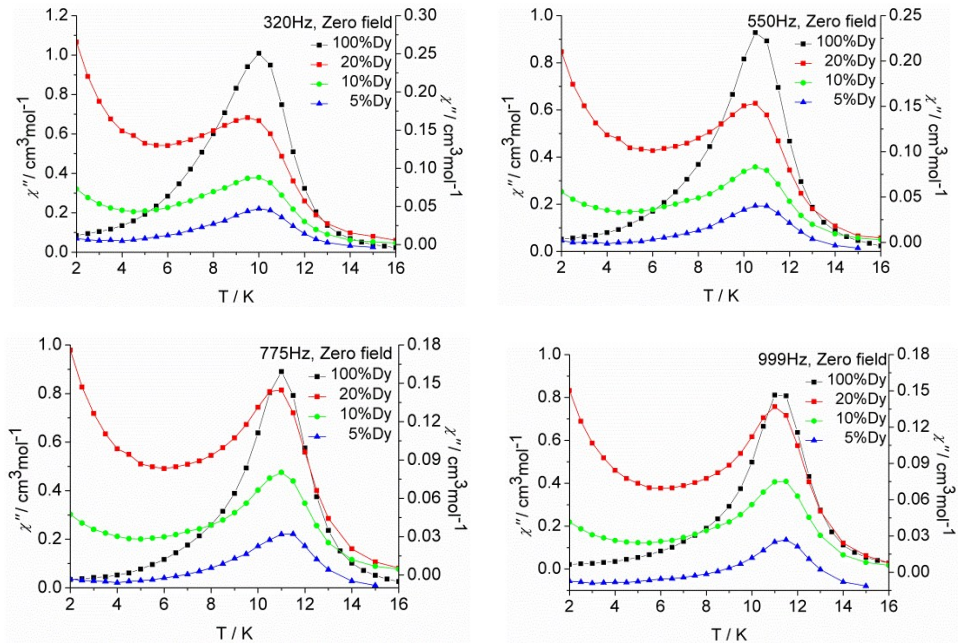


Fig. S15 Temperature dependence of the out-of-phase susceptibility (χ'') plot at indicated frequencies and 0 applied field on the diluted samples.

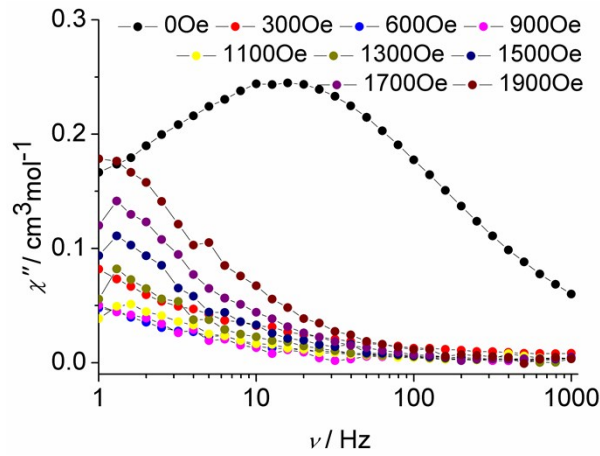


Fig. S16 Plot of the frequency dependence of the out-of-phase (χ'') ac susceptibility component under indicated dc field at 2 K for **1b**.

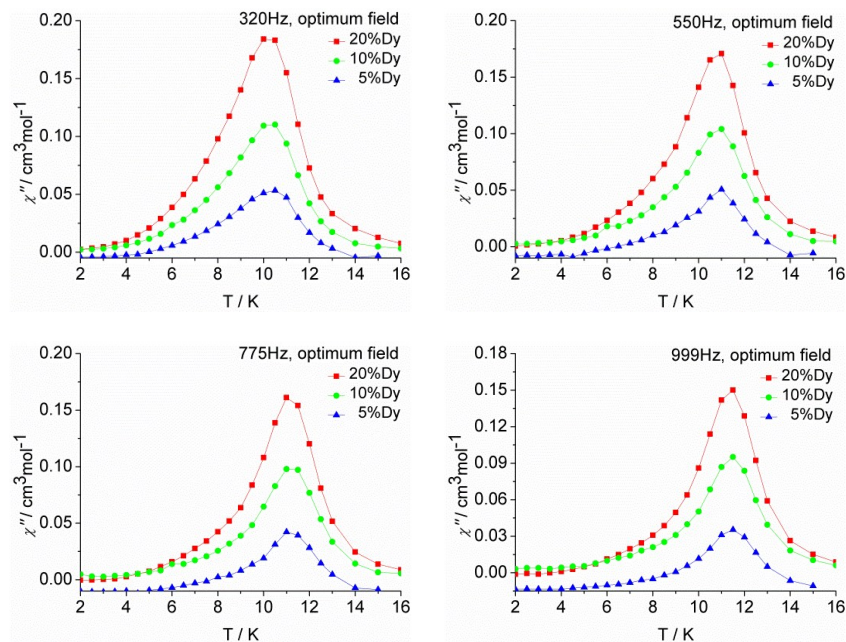


Fig. S17 Temperature dependence of the out-of-phase susceptibility (χ'') plot at indicated frequencies and applied field of 900 Oe on the diluted samples.

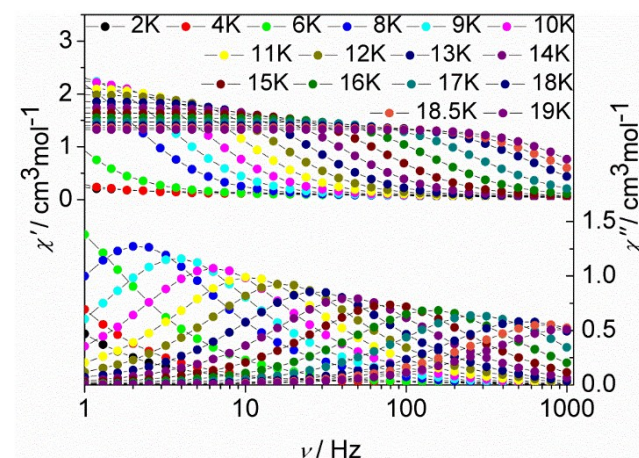


Fig. S18 Frequency dependence of the in-phase χ' and out-of-phase χ'' ac susceptibility signals under zero dc field at indicated temperatures for **de1**.

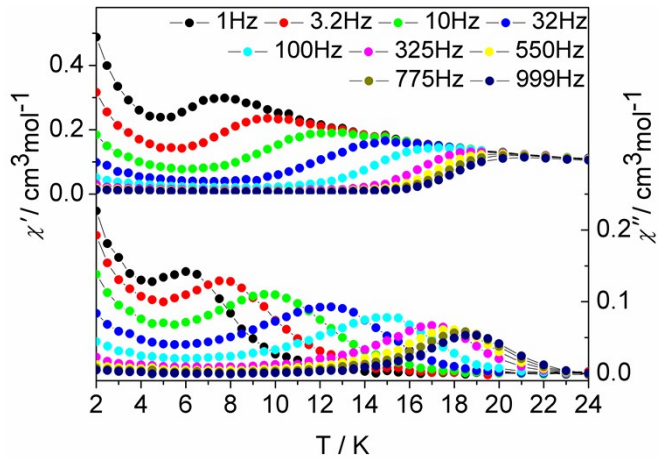


Fig. S19 Temperature dependence of the in-phase χ' and out-of-phase χ'' ac susceptibility signals under zero dc field for **de1b**.

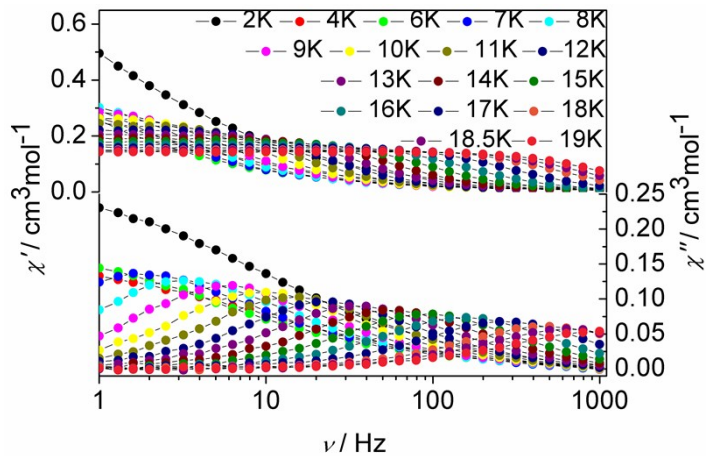


Fig. S20 Frequency dependence of the in-phase χ' and out-of-phase χ'' ac susceptibility signals under zero dc field at indicated temperatures for **de1b**.

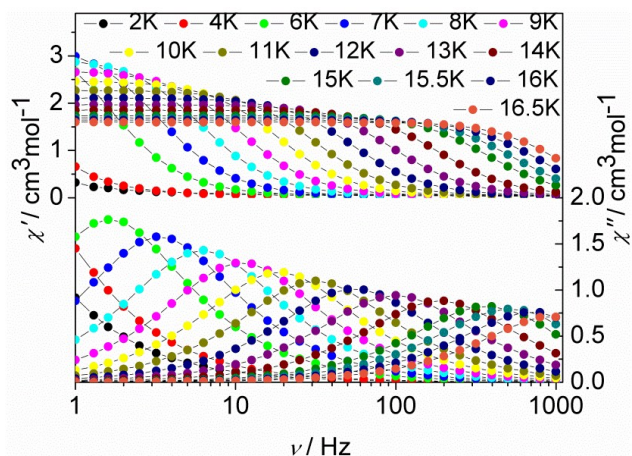


Fig. S21 Frequency dependence of the in-phase χ' and out-of-phase χ'' ac susceptibility signals under zero dc field at indicated temperatures for **2**.

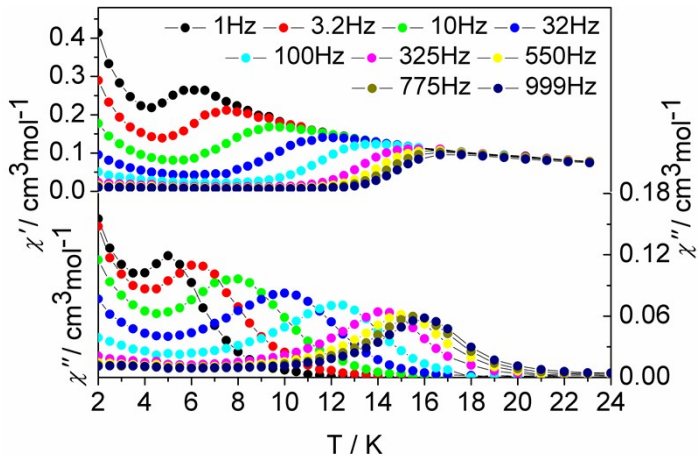


Fig. S22 Temperature dependence of the in-phase χ' and out-of-phase χ'' ac susceptibility signals under zero dc field for **2b**.

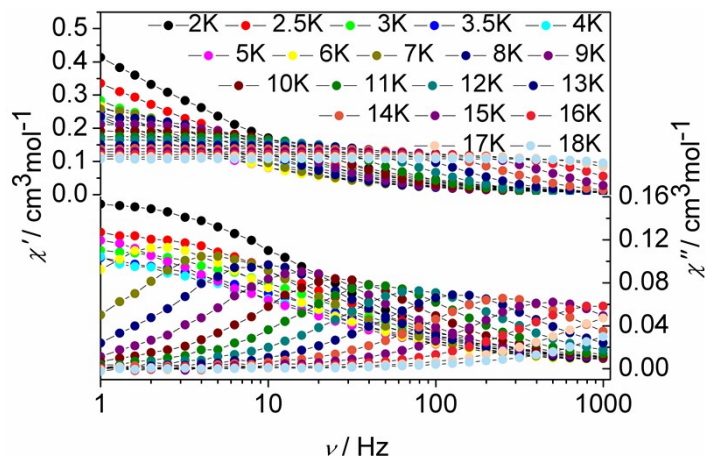


Fig. S23 Frequency dependence of the in-phase χ' and out-of-phase χ'' ac susceptibility signals under zero dc field at indicated temperatures for **2b**.

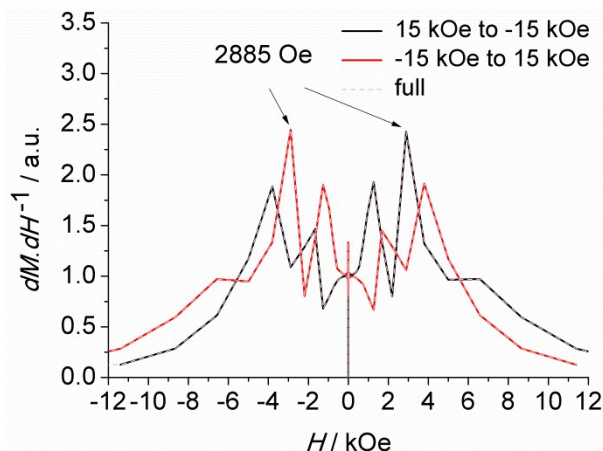


Fig. S24 The first derivative of magnetization (dM/dH) of complex **2** versus magnetic field for the curves measured at 1.8 K at scan rate of 200 Oe/s, sweep mode.

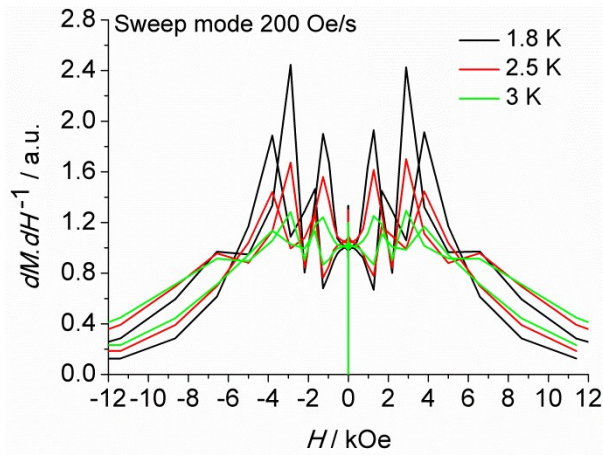


Fig. S25 The first derivative of magnetization (dM/dH) of complex **2** versus magnetic field for the curves measured at different temperature at scan rate of 200 Oe/s, sweep mode.

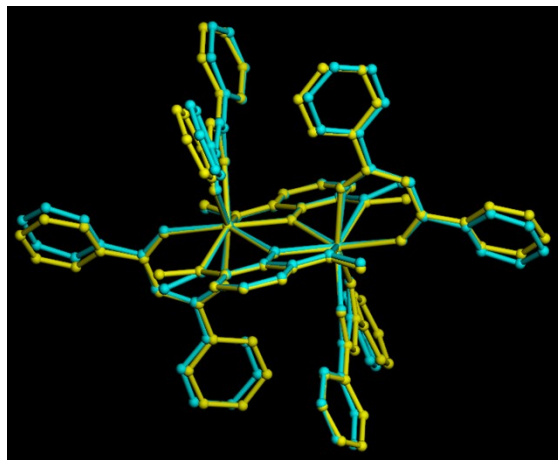


Fig. S26 The overlap plot for crystal structures of **1** (blue) and **2** (yellow).

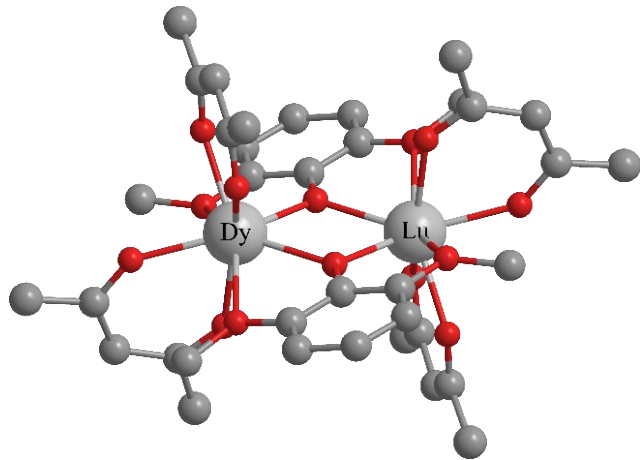


Fig. S27 Calculated model structure of complexes **1** and **2**.

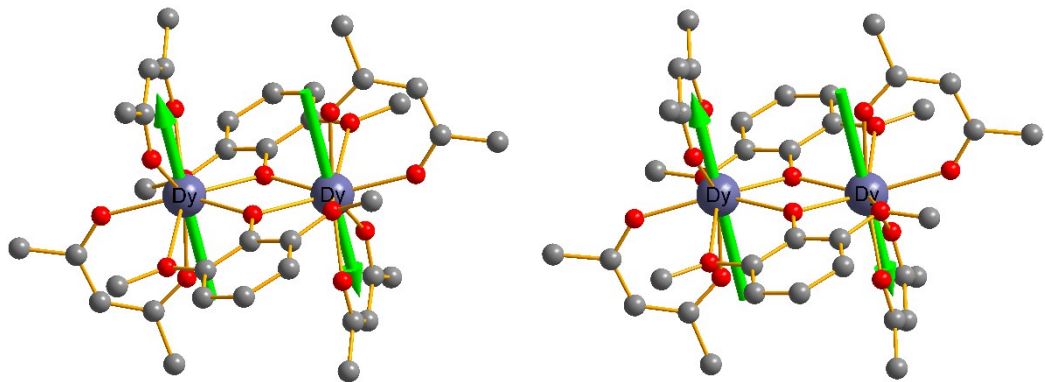


Fig. S28 Orientations of the local main magnetic axes of the ground doublets on Dy(III) ions of **1** and **2**.

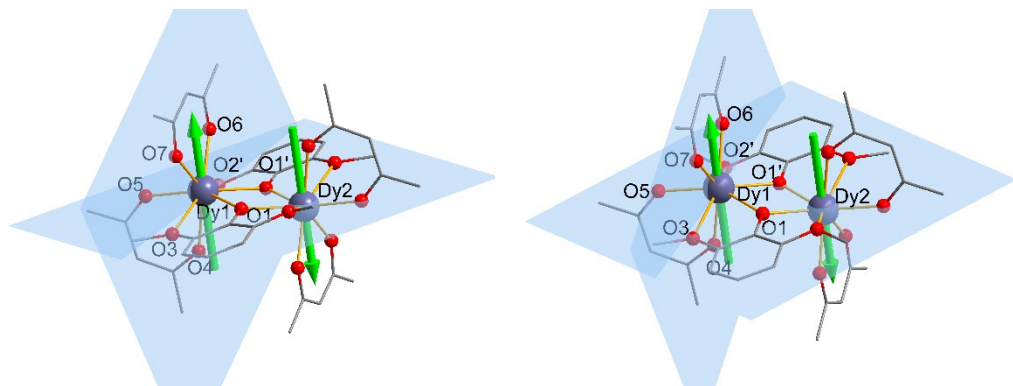


Fig. S29 Partially labeled crystal structure with the local main magnetic axes of the ground doublets on Dy(III) ions of **1** and **2**.

Table S1. Continuous Shape Measures (CShMs) of the coordination geometry for Dy(III) ion in compounds **1** and **2** (S values calculated with the Shape program). The S values indicated the proximity to the ideal polyhedron, thus, $S = 0$ corresponds to the non-distorted polyhedron. The three closer ideal geometries to the real complexes are listed and below are the symmetry and description for each polyhedron.

Compound	ideal geometries		$S_{\text{Dy}1}$	$S_{\text{Dy}1'}$
1	Biaugmented trigonal prism J50	C2v	2.288	2.285
	Biaugmented trigonal prism	C2v	2.657	2.656
	Triangular dodecahedron	D2d	3.337	3.332
2	Biaugmented trigonal prism J50	C2v	2.226	2.225
	Biaugmented trigonal prism	C2v	2.514	2.515
	Triangular dodecahedron	D2d	3.260	3.261

Table S2. Selected bond lengths (Å) and angles (°) for **1** and **2**.

	1		2
Dy1-O1	2.288(3)	Dy1-O1	2.2886(19)
Dy1-O1'	2.320(3)	Dy1-O1'	2.3140(18)
Dy1-O2'	2.621(3)	Dy1-O2'	2.6407(18)
Dy1-O3	2.696(3)	Dy1-O3	2.6319(18)
Dy1-O4	2.310(3)	Dy1-O4	2.296(2)
Dy1-O5	2.279(3)	Dy1-O5	2.280(2)
Dy1-O6	2.284(3)	Dy1-O6	2.286(2)
Dy1-O7	2.279(3)	Dy1-O7	2.279(2)
O1-Dy1'	2.320(3)	O1-Dy1'	2.3140(18)
O2-Dy1'	2.621(3)	O2-Dy1'	2.6407(18)
Dy1-Dy1'	3.8347(5)	Dy1-Dy1'	3.8452(3)
O1-Dy1-O1'	67.34(12)	O1-Dy1-O1'	66.68(7)
O1'-Dy1-O2'	63.88(10)	O1'-Dy1-O2'	64.15(6)
O1-Dy1-O2'	128.91(10)	O1-Dy1-O2'	129.33(6)
O1-Dy1-O4	91.05(11)	O1-Dy1-O4	88.89(7)
O1-Dy1-O3	63.43(10)	O1-Dy1-O3	64.72(6)
O1'-Dy1-O3	126.25(10)	O1'-Dy1-O3	126.61(7)
O5-Dy1-O1	145.22(12)	O5-Dy1-O1	145.46(6)
O6-Dy1-O1'	125.14(11)	O6-Dy1-O1'	126.54(7)
O7-Dy1-O1'	79.14(11)	O7-Dy1-O1'	81.40(7)
O4-Dy1-O1'	91.19 (11)	O4-Dy1-O1'	87.81(7)
O5-Dy1-O1'	141.73(11)	O5-Dy1-O1'	139.96(7)
O5-Dy1-O2'	78.26(11)	O5-Dy1-O2'	77.07(6)
O6-Dy1-O2'	139.32(12)	O6-Dy1-O2'	136.87(7)
O7-Dy1-O2'	70.94(11)	O7-Dy1-O2'	69.04(7)
O4-Dy1-O2'	75.90(12)	O4-Dy1-O2'	77.93(6)
O2'-Dy1-O3	144.11(11)	O2'-Dy1-O3	145.61(7)
O4-Dy1-O3	69.92(11)	O4-Dy1-O3	70.67(7)

O5-Dy1-O3	81.89(11)	O5-Dy1-O3	81.16(7)
O6-Dy1-O3	68.09(11)	O6-Dy1-O3	67.79(7)
O7-Dy1-O3	140.61(11)	O7-Dy1-O3	139.49(7)
O5-Dy1-O4	73.61(11)	O5-Dy1-O4	74.23(7)
O6-Dy1-O4	135.72(12)	O6-Dy1-O4	136.91(7)
O7-Dy1-O4	146.40(12)	O7-Dy1-O4	146.75(7)
O6-Dy1-O1	82.56(712)	O6-Dy1-O1	83.68(8)
O7-Dy1-O1	113.85(12)	O7-Dy1-O1	114.80(7)
O5-Dy1-O6	87.14(12)	O5-Dy1-O6	88.48(8)
O7-Dy1-O5	94.25(13)	O7-Dy1-O5	94.26(8)
O7-Dy1-O6	72.58(11)	O7-Dy1-O6	71.88(7)
Dy1-O1-Dy1'	112.66(12)	Dy1-O1-Dy1'	113.32(7)

Table S3. The bond lengths (\AA) of coordination polyhedron for **1** and **2**.

	1		2
O3-05	3.2753(42)	O3-05	3.2063(29)
O3-06	2.8095(45)	O3-06	2.7575(26)
O3-01	2.6435(55)	O3-01	2.6497(23)
O3-04	2.886(5)	O3-04	2.8634(39)
O5-06	3.1446(44)	O5-06	3.1852(30)
O1-06	3.0167(54)	O1-06	3.0512(32)
O5-04	2.7481(56)	O5-04	2.7614(29)
O1-04	3.2808(37)	O1-04	3.2104(27)
O1-01'	2.5534(47)	O1-01'	2.5296(34)
O7-06	2.7009(55)	O7-06	2.6790(38)
O5-07	3.3403(49)	O5-07	3.3410(27)
O5-02'	3.1025(62)	O5-02'	3.0785(37)
O4-02'	3.0413(47)	O4-02'	3.1162(29)
O4-01'	3.3074(49)	O4-01'	3.1970(27)
O2'-07	2.8569(40)	O2'-07	2.8035(33)
O7-01'	2.9295(43)	O7-01'	2.995(3)
O2'-01'	2.6274(42)	O2'-01'	2.6456(25)
O2'-03	5.0582(50)	O2'-03	5.0370(36)

Table S4. Selected Cl...H-C and C-H...pi interactions in **1** and **2** (\AA).

	1		2
Cl1...H22-C22_#1	4.076	Cl1...H4-C4_#7	3.595

Cl2...H8b-C8_#2	3.668	Cl1...H5-C5_#7	3.487
Cl3...H26-C26_#3	4.001	Cl1...H8b-C8_#8	3.578
Cl3...H27-C27_#3	3.864	Cl2...H5-C5_#7	3.855
Cl4...H23-C23	3.693	Cl2...H20-C20_#9	3.855
Cl4...H36-C36_#2	3.750	C39-H39...π(C9-C14)_#10	3.541
Cl5...H13-C13_#4	3.788		
Cl6...H8c-C8_#5	3.862		
Cl6...H20-C20_#6	3.812		
C39-H39...π(C33-C38)_#2	3.619		
C40-H40...π(C24-C29)	3.505		

Symmetry transformations used to generate equivalent atoms: #1: 1-x, 1-y, z; #2: 1-x, 1-y, 1-z; #3: x-1, y, z; #4: 1-x, -y, -z; #5: x, y, z-1; #6: 1+x, y, z; #7: x, y-1, 1+z; #8: -x, 1-y, 1-z; #9: 1-x, -y, 1-z; #10: x, y, z+1.

Table S5. Parameters of the magnetic interactions between Dy(III) ions in **1** and **2** (cm⁻¹).

	J_{dip}	J_{ex}	J_{total}
1	-2.77	-1.25	-4.02
2	-2.51	-3.00	-5.51

Table S6. Best fitted parameters (χ_T , χ_S , τ and α) with the extended Debye model for complex **1** at 0 Oe in the temperature range 2-12 K.

T/ K	$\chi_S / \text{cm}^3 \text{ mol}^{-1}$	$\chi_T / \text{cm}^3 \text{ mol}^{-1}$	τ/s	α
2	0.03660	4.70620	0.06436	0.18615
2.25	0.02936	4.90060	0.05960	0.18525
2.5	0.03307	4.88062	0.05235	0.17135
2.75	0.02587	4.80125	0.06647	0.19720
3	0.04017	4.70482	0.03984	0.14217
3.25	0.04569	4.61686	0.03485	0.13122
3.5	0.03054	4.60073	0.03099	0.13363
3.75	0.04454	4.40013	0.02594	0.11002
4	0.04667	4.24332	0.02196	0.09780
4.5	0.04957	4.00242	0.01585	0.08045

5	0.04937	3.75822	0.01145	0.06812
5.5	0.05086	3.54566	0.00840	0.05883
6	0.04715	3.34893	0.00617	0.05182
6.5	0.04688	3.17276	0.00463	0.04921
7	0.05207	3.01268	0.00352	0.04491
7.5	0.04415	2.86711	0.00270	0.04693
8	0.04151	2.74297	0.00209	0.04617
8.5	0.09891	2.61971	0.00165	0.03104
9	0.09510	2.50036	0.00126	0.03564
9.5	0.04097	2.39645	0.00091	0.05768
10	0.05590	2.29916	0.00063	0.06079
10.5	0.07437	2.20597	0.00042	0.06963
11	0.10181	2.12711	0.00026	0.08851
11.5	0.20657	2.04635	0.00016	0.10795

Table S7. The curves are fitted by the modified Arrhenius relationship in which the QTM and Raman processes are taken account

$$1/\tau = 1/\tau_{\text{QTM}} + CT^n + \tau_0^{-1} \exp(-U_{\text{eff}}/\kappa T)^2$$

complex	q (s)	C ($\text{s}^{-1} \cdot \text{K}^{-n}$)	n^3	τ_0 (s)	U_{eff}/k_B (K)
1	7.3×10^{-2}	0.16	3.8	2.5×10^{-6}	157.2
2	8.4×10^{-1}	1.4×10^{-3}	4.9	2.0×10^{-9}	190.8
de1	3.7×10^{-1}	1.2×10^{-4}	5.5	2.4×10^{-10}	258.4

Table S8. Dy(III)-Dy(III) coupling constant (cm^{-1} , in the $-J$ form) in **2** obtained by two different method.

Method	J_{dip}	J_{ex}	J
Level-crossing	-2.51	-2.81	-5.32
POLY_ANISO	-2.51	-3.00	-5.51

² The Equation consider the spin-lattice relaxation of Raman, Orbach and QTM processes, where τ_{QTM} is the QTM relaxation time, C is the coefficient of Raman process, U_{eff} is the energy barrier to magnetization reversal and k_B is the Boltzmann constant.

³ In general, $n = 9$ is rational for Kramers ions, but when both the acoustic and optical phonons are considered depending on the structure of energy levels, n values between 1 and 6 are reasonable.^{S3}

Computational details

There are one types of Dy(III) ion for each of complexes **1** and **2**, and thus we only need to calculate one Dy(III) fragments for each of them. Complete-active-space self-consistent field (CASSCF) calculations on individual lanthanide Dy(III) fragment of the model structure ([Fig. S27](#) for the model structure of complexes **1** and **2**) extracted from complexes **1** and **2** on the basis of X-ray determined geometry have been carried out with MOLCAS 7.8 program package.^{S4}

During the calculations, the other Dy(III) ions for each complex were replaced by diamagnetic Lu³⁺. The basis sets for all atoms are atomic natural orbitals from the MOLCAS ANO-RCC library: ANO-RCC-VTZP for Dy(III) ions; VTZ for close O; VDZ for distant atoms. The calculations employed the second order Douglas-Kroll-Hess Hamiltonian, where scalar relativistic contractions were taken into account in the basis set and the spin-orbit couplings were handled separately in the restricted active space state interaction (RASSI-SO) procedure. For the fragment of Dy(III), active electrons in 7 active spaces include all *f* electrons (CAS(9 in 7) in the CASSCF calculation. We have mixed the maximum number of spin-free state which was possible with our hardware (all from 21 sextets, 128 from 224 quadruplets, 130 from 490 doublets for the Dy(III) fragment).

To fit the exchange interactions in two complexes, we took two steps to obtain them. Firstly, we calculated one Dy(III) fragment using CASSCF to obtain the corresponding magnetic properties. And then, the exchange interaction between the magnetic centers is considered within the Lines model,^{S5} while the account of the dipole-dipole magnetic coupling is treated exactly. The Lines model is effective and has been successfully used widely in the research field of f-element single-molecule magnets.^{S6}

For each of complexes **1** and **2**, there is only one type of *J*. The intermolecular interactions *zJ'* of **1** and **2** were set to 0.00 cm⁻¹ and 0.11 cm⁻¹, respectively.

The exchange Hamiltonian is:

$$\hat{H}_{exch} = -J^{total} \hat{\mathcal{S}}_{B_y1} \hat{\mathcal{S}}_{B_y2} \quad (S2)$$

The *J*^{total} is the parameter of the total magnetic interaction (*J*^{total} = *J*^{dipolar} + *J*^{exchange}) between magnetic center ions. The $\hat{\mathcal{S}}_{B_y} = \pm 1/2$ are the ground pseudospin on the Dy(III) sites. The dipolar magnetic coupling can be calculated exactly, while the exchange coupling constants were fitted

through comparison of the computed and measured magnetic susceptibility and molar magnetization using the POLY_ANISO program.^{S7}

Table S9. Energies (cm⁻¹) and *g* (*g_x*, *g_y*, *g_z*) tensors of the lowest spin-orbit states on one Dy(III) fragment of **1** and **2**.

1		2	
Energy of eight lowest KDs	<i>g</i> tensor of the ground KD	Energy of eight lowest KDs	<i>g</i> tensor of the ground KD
0.0	<i>g_x</i> = 0.008	0.0	<i>g_x</i> = 0.004
106.7	<i>g_y</i> = 0.028	134.3	<i>g_y</i> = 0.016
196.3	<i>g_z</i> = 19.769	206.7	<i>g_z</i> = 19.778
252.4		280.1	
292.7		315.2	
347.0		358.9	
393.9		413.9	
580.2		593.7	

Table S10. Exchange energies (cm⁻¹) and main values of the *g_z* for the lowest two exchange doublets.

1		2		
	<i>E</i>	<i>g_z</i>	<i>E</i>	<i>g_z</i>
1	0.0	0.000	0.0	0.000
2	1.9	39.537	2.7	39.553

References:

- S1 W. Plass and G. Fries, *Allg. Chem.*, 1997, **623**, 1205.
- S2 P. Comba, M. Großhauser, R. Klingeler, C. Koo, Y. Lan, D. Müller, J. Park, A. Powell, M. J. Riley and H. Wadeohl, *Inorg. Chem.*, 2015, **54**, 11247.
- S3 K. N. Shirivastava, *Phys. Status Solidi B*, 1983, **117**, 437.
- S4 G. Karlström, R. Lindh, P.-Å. Malmqvist, B. O. Roos, U. Ryde, V. Veryazov, P.-O. Widmark, M. Cossi, B. Schimmelpfennig, P. Neogrady, L. Seijo, *Comput. Mater. Sci.* 2003, **28**, 222.

S5 M. E. Lines, *J. Chem. Phys.*, 1971, **55**, 2977.

S6 (a) K. C. Mondal, A. Sundt, Y. H. Lan, G. E. Kostakis, O. Waldmann, L. Ungur, L. F. Chibotaru, C. E. Anson and A. K. Powell, *Angew. Chem. Int. Ed.*, 2012, **51**, 7550; (b) S. K. Langley, D. P. Wielechowski, V. Vieru, N. F. Chilton, B. Moubaraki, B. F. Abrahams, L. F. Chibotaru, K. S. Murray, *Angew. Chem. Int. Ed.*, 2013, **52**, 12014.

S7 (a) L. F. Chibotaru, L. Ungur and A. Soncini, *Angew. Chem. Int. Ed.*, 2008, **47**, 4126; (b) L.; Ungur, W. V. den Heuvel, L. F. Chibotaru, *New J. Chem.*, 2009, **33**, 1224; (c) L. F. Chibotaru, L. Ungur, C. Aronica, H. Elmoll, G. Pilet and D. Luneau, *J. Am. Chem. Soc.*, 2008, **130**, 12445.